Knowledge-based Engineering and Sciences (2024), **5**, (3), 83–101
doi:10.51526/kbes.2024.5.3.83-101

RESEARCH PAPER

Utilization of Doum Shell Catalyst in Biodiesel Production from Palmitic Acid: Development of Statistical Optimization Approach

Haruna Mavakumba Kefas,*[,1] Jerome Undiandeye,[2] Abdulhalim Musa Abubakar,*[,1] and Benjamin John[1]

[1]Department of Chemical Engineering, Faculty of Engineering, Modibbo Adama University, P.M.B. 2076, Yola, Adamawa State, Nigeria
[2]Department of Chemical Engineering, Faculty of Engineering, University of Port Harcourt (UNIPORT), Rivers State, Nigeria
*Corresponding author. Email: hmkefas@mau.edu.ng; abdulhalim@mau.edu.ng

(Received 06 September 2024; revised 29 November 2024; accepted 29 December 2024; first published online 31 December 2024)

Abstract

One specific advantage of using palmitic acid (PA) in biodiesel (Fatty Acid Methyl Esther, FAME) production is its availability and high cetane number. To produce FAME, the methodological steps followed in this study involved the sourcing and preparation of doum palm shell (DPS), carbonization and sulfonation of the biochar, and subsequent esterification of PA while DPS serves as catalyst. The objectives are to systematically explore the catalytic potential of DPS to optimize the biodiesel conversion by varying some process parameters, including methanol/oil ratio (8:1 to 12:1), reaction time (60–180 min) and catalyst load (1–5 wt.%). Ab initio, a Fourier Transform Infrared (FTIR) spectroscopy of the prepared DPS catalyst and char revealed the presence of sulfonic acid groups crucial for enhancing the acidic nature and catalytic activity of the catalyst, as well as the carbonyl groups which facilitates the esterification reaction. A sister characterization method known as the Atomic Force Microscopy (AFM) suggest that the biomass catalyst has a moderately rough surface with substantial peaks and valleys, that enhance FAME conversion. Later on, several statistical metrics, 3D surface plot, contour lines, fitted plot and a quadratic model relating the 3 factors and the response, helped in the selection of optimal combination. Under 100% desirability corresponding to 97.83% biodiesel conversion, Design Expert 7.0.0 points to 4.24 wt.%, 10.57:1 and 126.67 min as optimal combinations of catalyst load, methanol–oil ratio and reaction time, respectively, also in line with a validated experimental efficiency of 98.01%. Based on the aforementioned meritorious properties of the PA and DPS used, a biodiesel with better oxidative stability, lower levels of polyunsaturated fatty acids, longer shelf life and improved performance in diesel engines, is expected.

Keywords: Palmitic acid; Biodiesel optimization; Doum shell; Sulfonation; Esterification.

1. Introduction

A systematic exploration of alternative catalysts for biodiesel (FAME) production is crucial for developing more efficient and sustainable energy sources. Doum palm shell (DPS) and related extract were previously used as adsorbent [1], [2], [3]; as reinforcement material [4], [5], [6], [7], [8] and; investigated for their thermal properties [9], [10], [11]. DPS utilization as a catalyst in biodiesel

production represents a novel approach that is poised at addressing several gaps in previous research. While significant work has been conducted on various feedstock and catalysts, the potential of DPS, particularly when sulfonated, was brought to limelight in a study [12]. Transesterification, though widely used, poses challenges such as the need for high-quality feedstock with low free fatty acid (FFA) content and the formation of soap [13], which complicates the process. Esterification, on the other hand, can directly convert FFAs into biodiesel, making it more suitable for feedstock with high FFA content. A closer inclination to the use of DPS for biofuel production [14], reported the kinetics and thermodynamic study of the pyrolysis step. Palmitic acid (PA – hexadecanoic acid), a saturated fatty acid prevalent in many oils and fats, is significant due to its abundance and ease of conversion into FAME. The presence of PA in various feedstock offers a reliable source for biodiesel production, especially when efficient catalysts like the DPS catalyst are used. PA is produced through several methods, primarily involving extraction from natural sources such as animal fats (lard, tallow) and plant oils (palm oil, palm kernel oil, coconut oil). It can also be synthesized chemically via hydrolysis of triglycerides, where fats and oils are broken down with water, heat, and a catalyst, or through hydrogenation of unsaturated fats. Industrial production methods include fractionation and distillation of fatty acids from palm oil [15] and various oleochemical processes that modify natural oils and fats to isolate and purify PA. These methods ensure a reliable supply of PA for diverse applications, including food, cosmetics and biodiesel production. Doum palm (*Hyphaenethebaica*) is native to various regions and can be found in countries such as Egypt, Sudan, Nigeria, Chad, Mali, Niger, Somalia, Kenya, Tanzania, Senegal, and Ethiopia. Among them, Sudan is recognized as the largest producer of doum palm. These countries, predominantly located in North and East Africa, provide environments conducive to the growth of the doum palm, making the DPS readily available for use in various applications, including as a catalyst in biodiesel production.

Fourier Transform Infrared Spectroscopy (FTIR) analysis usually reveal the presence of sulfonic acid groups, which are critical for enhancing the acidic nature and catalytic activity of the catalyst. These functional groups play a vital role in facilitating esterification reactions by providing active sites for proton donation. Moreso, characterizing the DPS catalyst by Atomic Force Microscopy (AFM) will reveal the surface morphology and roughness of the catalyst [16]. Normally, an increased surface area enhances catalytic activity by providing more active sites for reaction. Hence, this research aims to solve the absence of an optimized FAME production in the literature using a sulfonated DPS catalyst, in the esterification of PA. Ideally, the optimization of the biodiesel production process can be conducted using Design Expert and Central Composite Design-Response Surface Methodology (CCD-RSM) [17], [18], [19], [20], [21]. A detailed description of the application of CCD in optimization have been presented [22]. This approach allowed for the systematic variation and optimization of critical process parameters, including methanol/oil ratio, reaction time, and catalyst load. These factors are pivotal in determining the efficiency of the esterification process [23], [24]. An optimal methanol/oil ratio ensures sufficient methanol is available for the reaction, while appropriate reaction times and catalyst loads maximize conversion rates without unnecessary resource expenditure. The significance of finding the optimal conditions for these parameters cannot be overstated. Achieving high biodiesel conversion rates ensures the process is economically viable and scalable. The use of DPS as a catalyst not only provides a sustainable solution but also leverages local resources, reducing dependency on conventional catalysts and enhancing the overall sustainability of FAME production. Therefore, the objectives of this study are to explore the potential of sulfonated DPS as a catalyst for the esterification of PA and to optimize key process parameters using advanced methodologies to enhance the efficiency and sustainability of biodiesel production. The main interest in using DPS in biodiesel production lies in its high catalytic activity due to sulfonation, which provides abundant acidic sites for esterification and transesterification. Because it enhances reaction efficiency, aligns with the chemical mechanism and effectively converts PA into FAME through proton donation and stabilization of intermediates.

2. Materials and method

The entire study was guided by the designed flow chart shown in Figure 1. It depicts the basic steps involved in the production of FAME and the optimization study proper.

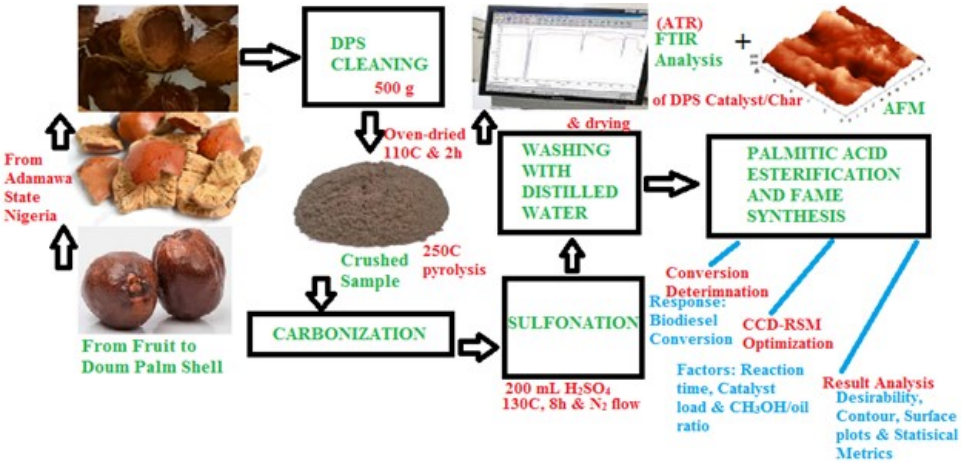

Figure 1: *Modelled Experimental and Result Analysis Flowchart.*

2.1 DPS Sourcing

Already, studies have proven the relative availability of doum palm fruit in Nigeria [25], [26]. Doum palm shell (DPS) was locally gotten from a farm in Yola metropolis. Yola is located between latitude 9.2035°N and longitude 12.4954°E in Adamawa State, North-East, Nigeria. It was cleaned and processed prior to its subsequent utilization.

2.2 Carbon Based Sulfonated Catalyst (CBSC) Preparation

About 500g of DPS was cleaned, crushed and put into a container. It was then placed in an oven for 2 h at 110°C to eliminate its water content. CBSC was prepared by a two-step process: carbonization and sulfonation. First, DPS was obtained and pyrolyzed in a tube furnace under inert condition at 250°C for 1.5 h. It was quenched with water and allowed to cool at room temperature. The resultant char also obtained was ground using a pestle and mortar into fine powder [27]. Precisely, 20g of the DPS biochar was sulphonated in a 3-necked round bottom flask using 200 mL of fuming sulfuric acid (H_2SO_4) at 130°C for 8 h under nitrogen (N_2) flow, with a constant mixing using magnetic stirrer at 600 rpm, in semblance [28]. After cooling to room temperature, the sulfonated DPS was washed with distilled water filtered using suction pump and oven-dried at 105°C for 15h. The washing of the sulfonated char was carried out to remove excess sulphate ions.

2.3 FTIR Spectroscopy of DPS-CBSCs

Chemical composition of the CBSC solid residues before and after the pre-treatments were analyzed by attenuated total reflection–(ATR-FTIR). ATR-FTIR was conducted using a Thermo scientific PIKE Nicolet IS5, with built-in diamond-germanium ATR single reflection crystal. Samples were pressed firmly against the diamond surface using a screw-loaded anvil. Sample spectra were obtained using 32 scans in the wave number range of 650-4000 cm^{-1} at a spectral resolution of 4 cm^{-1}.

2.4 AFM for Nanoparticle Characterization

AFM version 3.8.1.9 was used so as to obtain a 3D characterization of nanoparticles with sub-nanometer resolution. Nanoparticle size distributions were directly calculated from the AFM images.

2.5 Esterification of Palmitic Acid

PA esterification reaction was carried out using the conventional reflux method. As used by researchers, a 250 mL of three-necked round bottom flask was used and sub immersed in an oil bath [29], [30]. The condenser was coupled with round bottom flask to re-condense the evaporated methanol (CH_3OH). Essentially, 3 g of PA was mixed with the calculated amount of CH_3OH and catalyst. The suspension was then refluxed at a certain temperature with a stirring speed of 600 rpm, faster, but close to 660 rpm optimal value reported [31]. Based on the procedure described [32], the catalyst was separated from the suspension by centrifugation for 5 min, at the end of the process. The CH_3OH was then separated and recovered from the product. Lastly, the separated product (PA methyl ester – FAME) was collected.

2.6 Computation of FFA Conversion

FFA conversion of the PA was calculated based on the difference between the acid value of the feedstock and acid value of the product. This FFA was according to Equation 1 (AOCS 5a-40 standard method) [30, 34]. The biodiesel conversion (%) was computed for several runs using Equation 2 [33].

$$\text{FFA Conversion (\%)} = \frac{AV_f - AV_p}{AV_f} \times 100 \tag{1}$$

$$\text{Biodiesel Conversion (\%)} = \frac{\text{FFA}_f - \text{FFA}_p}{\text{FFA}_f} \times 100 \tag{2}$$

Where, AV_f and AV_p stands for the acid value of the feedstock and acid value of the product, respectively, and FFA_f and FFA_p are FFA of the feed and the product, respectively.

2.7 Biodiesel Optimization using RSM

Process variables including methanol-oil ratio, reaction time and catalyst load were varied from 8:1 to 12:1, 60-180 min and 1-5 wt.% (Table 1), respectively in order to determine the optimal combination for a higher FAME production using RSM. Briefly, RSM is a statistical and mathematical technique used to model and analyze the relationships between multiple independent variables and one or more response variables. It is particularly useful for optimizing processes by developing a functional relationship through designed experiments and visualizing interactions via response surfaces. It is worthy of note that the molar ratio used herein was an arbitrary range, due to the fact that lower (4:1 to 8:1 3:1 to 9:1) or higher (13:1 34:1) range can also be experimented [34], [35], [36], [37]. The variables was based on a reaction temperature of 65°C used [38], because conventional range reported in the literature is 55-65°C [12, 41, 42]. In the Design Expert tool, the factors were named A, B and C; standing for methanol-oil ratio, reaction time and catalyst load, respectively.

Table 1: *Range of the Selected Process Variable for Biodiesel Optimization*

Factor	Low Actual	High Actual	Low Coded	High Coded	Mean	Std. Dev.
A	8	12	-1	1	10	1.414214
B	60	180	-1	1	120	42.42641
C	1	5	-1	1	3	1.414214

Automatically, the mean and standard deviation for the respective minimum and maximum data entrance were computed and recorded, as shown in Table 1.

2.8 Design of Experiment and Statistical Analysis

In the Design Expert 7.0.0 application, a Study Type 'Response Surface', Randomized Subtype and a Quadratic Design Model were initiated for 20 runs of Central Composite Design (CCD) data and an Import Data Design Type (User-defined). This is expected to give a table of predicted results called design of experiment (DOE) for the 3 factors and 1 response (biodiesel conversion). A second order quadratic model was acquired to describe the precise correlation between the response and the independent variables [41]. The empirical correlation between the biodiesel conversion (%) in terms of coded independent factors was obtained and the statistical analysis of the model was evaluated using analysis of variance (ANOVA).

Essentially, Factorial Design (Fact) was used to explore main effects of factors A, B, and C, as purely employed in 30 runs DOE [42]. Axial Design or 'Axial' tests the robustness of the optimal conditions found in the factorial design; while the Central Composite Design (Center), explores the response surface more thoroughly around the optimal conditions identified. Practically, the total number of experiments conducted was $20(= 2^k + 2k + 6)$ [43], where k is the number of independent variables, including 8 factorial points, 6 axial points and 6 center points. Further analysis, through statistical modeling like regression or optimization algorithms, was explored to identify optimal conditions for maximizing FAME conversion while considering resource efficiency and environmental impact.

3. Result and dicussion

3.1 FTIR Images

FTIR analysis of the DPS catalyst (Figure 2a) and DPS biochar (Figure 2b) reveals distinct differences and similarities in the functional groups present, which significantly impact their performance as catalysts in biodiesel production. Both FTIR spectra exhibit peaks corresponding to similar functional groups, indicating the presence of common chemical structures. Key functional groups observed in both spectra include: O-H stretching broad peaks around 3200-3600 cm^{-1} indicating hydroxyl groups, which are present in both catalysts [3]; C-H stretching peaks around 2800-3000 cm^{-1} corresponding to aliphatic C-H stretching vibrations, signifying the presence of methyl and methylene groups [44]; C=O stretching sharp peaks around 1700 cm^{-1} suggest the presence of carbonyl groups [33], which are crucial in the catalytic activity for esterification reactions and; C-O stretching peaks in the range of 1000-1300 cm^{-1} are indicative of C-O stretching vibrations [45], associated with alcohols, esters, and carboxylic acids.

However, there are notable differences between the two spectra. First, the DPS catalyst shows strong peaks around 1000-1200 cm^{-1}, which correspond to sulfonic acid groups (S=O stretching). These peaks are less pronounced or absent in the DPS biochar. Secondly, peaks around 1500-1600 cm^{-1} in the DPS biochar indicate aromatic C=C stretching vibrations [46], which are less prominent in the DPS catalyst. The presence of different functional groups in the DPS catalyst and DPS biochar affects their efficiency in biodiesel production. For instance, the presence of S=O stretching significantly enhances the acidic properties of the DPS catalyst, making it more effective in catalyzing the esterification and transesterification reactions crucial for biodiesel production. The acidic nature of sulfonic groups facilitates proton donation [32], improving the conversion rates of FFAs to FAME. While the DPS biochar contains essential functional groups like carbonyl (C=O) and hydroxyl groups (–OH), the absence or lower intensity of sulfonic acid groups reduces its catalytic efficiency compared to the DPS Catalyst. The aromatic structures present in the biochar (specifically, –OH) may contribute to adsorption processes as reported [47], but do not provide the same level of catalytic activity as the sulfonated catalyst.

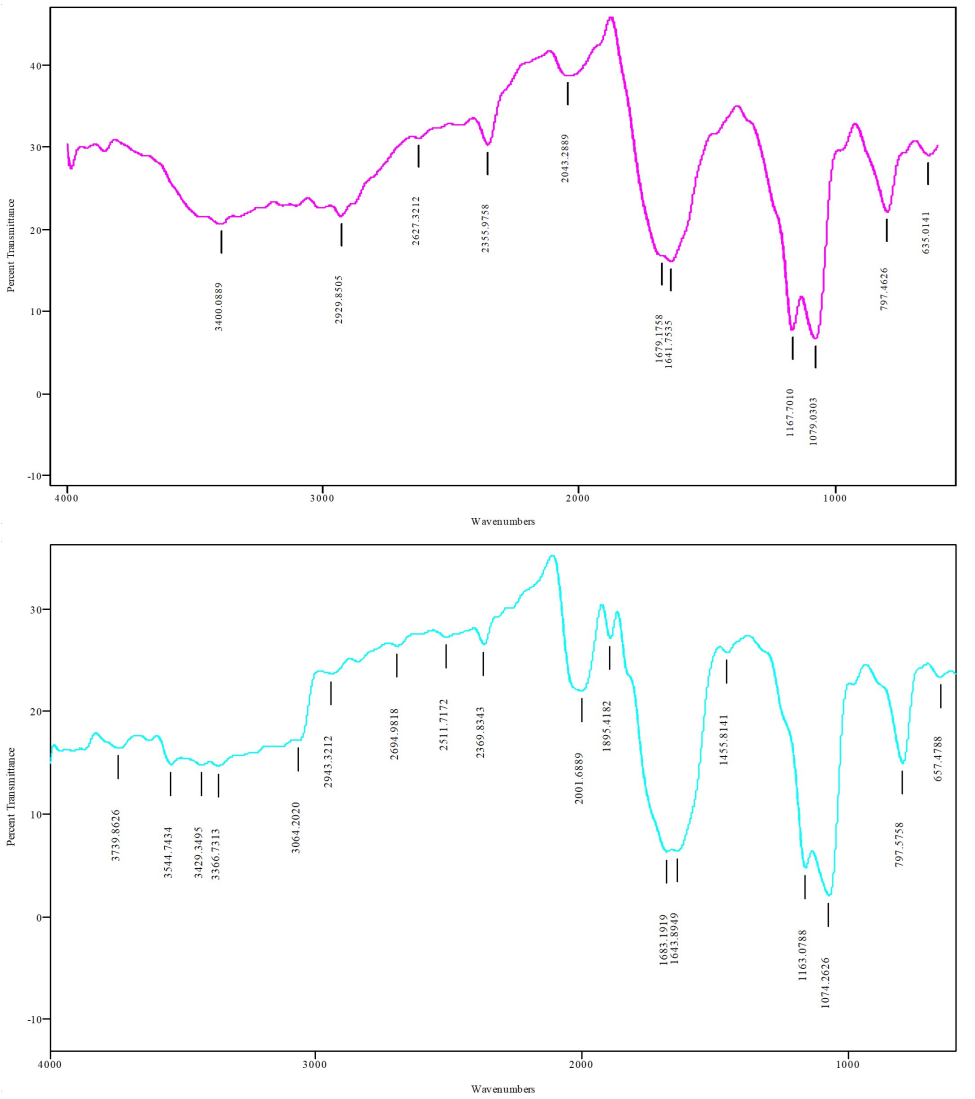

Figure 2: *DPS (a) Catalyst and (b) Biochar IR Spectroscopy.*

3.2 AFM Images

Atomic Force Microscopy (AFM) analysis of the Doum Shell Catalyst (DSC), as shown in Figure 3, provides critical info into its surface morphology and topographical characteristics, which are vital for its application in FAME production. The AFM specifications reveal several important parameters. An area roughness (Sa) is 2595.4 picometers (pm), indicating a relatively smooth surface at the nanometer scale. Root mean square roughness (Sq) is 3.4124 nanometers (nm), and the maximum peak-to-valley height (Sy) is 19.203 nm. As described in research, these values suggest that the DSC has a moderately rough surface with significant peaks and valleys [48]. The specific scan details, such as an image size of 50 μm, scan direction (up and down), and the resolution (239 points and lines), ensure a high-resolution analysis capable of detecting minute surface variations.

In the context of biodiesel production, the surface roughness and topography of the DSC are crucial. A higher surface roughness increases the surface area available for catalytic reactions, thereby

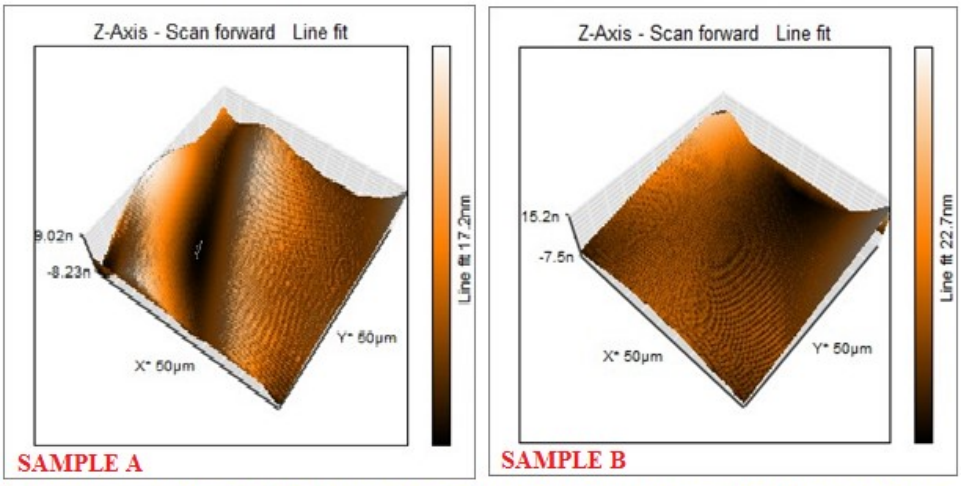

(a) 3-D View of Doum Shell Catalyst Before AFM **(b) 3-D View of Doum Shell Catalyst After AFM**

Figure 3: *Doum Shell Catalyst AFM.*

enhancing the catalytic activity. Presence of significant peaks and valleys on the catalyst surface provides more active sites for the adsorption and conversion of reactants into FAME. This increased surface area and the presence of active sites are particularly beneficial in the esterification and transesterification reactions involved in biodiesel production. Furthermore, the specific approach parameters, such as the setpoint of 20 nanonewtons (nN) and the adaptive PID feedback algorithm, ensure that the AFM analysis is precise and accurate, providing reliable data on the catalyst's surface characteristics. The use of static force operating mode and the specific cantilever type (XYCONTR) are also optimized for high-resolution imaging of the catalyst's surface, allowing for detailed analysis of its morphological features [49].

3.3 RSM Model Statistics

Prior to the forgone analysis, runs 6, 7, 10, 16 and 18 consistently show high conversion rates, suggesting robust conditions for high biodiesel conversion, as shown in Table 2.

Sum of squares (SS) quantifies the variation in the response variable (i.e., FAME conversion) that can be attributed to each source. For example, "Mean vs Total" has the highest SS (173,976.5), indicating the total variability in the data. On the other hand, "Linear vs Mean" has an SS of 258.98, showing the contribution of linear terms to the model, as shown in Table 3. It is worthy of note that the degrees of freedom (df) reflect the number of independent values that can vary. A "Residual" df of 6 indicates the number of independent pieces of information available to estimate the model's error. The mean square (MS) is SS divided by the corresponding df [50]. For the "Quadratic vs 2FI," the MS is 54.21 (Table 2), which is relatively high, indicating a significant contribution to the model.

F value tests the overall significance of the model, in which a higher F value indicates a more significant contribution. Viz., "Quadratic vs 2FI" has an F value of 189.63, with a p-value < 0.0001, suggesting a highly significant quadratic term. Normally, p-values indicates the probability that the observed results are due to chance. A p-value < 0.05 generally indicates statistical significance [51]. Here (in Table 3), the "Linear vs Mean" term has a p-value of 0.0017, and the "Quadratic vs 2FI" term has a p-value of < 0.0001 [52], both indicating strong statistical significance. Conversely, the "2FI vs Linear" term has a p-value of 0.9386, showing it is not significant. In Table 4, the lack of fit tests evaluates the adequacy of different model types in representing the data [53]. The quadratic

model has an SS of 2.357781, MS of 0.471556, an F value of 4.70474, and a p-value of 0.0572. This p-value is slightly above the conventional significance level of 0.05, suggesting that the lack of fit is not significant, as realized [54]. This indicates that the quadratic model provides an adequate fit to the data, making it a suitable choice for modeling the system under study. The cubic model, while having a lower SS (1.270381), presents a significant lack of fit with an F value of 12.67466 and a p-value of 0.0162, implying overfitting and thus is aliased.

Table 2: *Experimental Designs Generated by RSM and the Response for Each Reaction Run.*

Std	Run	Type	Factor A	Factor B (min)	Factor C (wt.%)	Response 1
1	1	Fact	8	60	1	82.59
2	2	Fact	12	60	1	85.03
12	3	Axial	10	180	3	94.87
11	4	Axial	10	60	3	91.05
20	5	Center	10	120	3	96.98
10	6	Axial	12	120	3	97.7
17	7	Center	10	120	3	96.47
7	8	Fact	8	180	5	97.17
9	9	Axial	8	120	3	96.47
6	10	Fact	12	60	5	94.45
8	11	Fact	12	180	5	95.54
13	12	Axial	10	120	1	86.59
16	13	Center	10	120	3	96.55
15	14	Center	10	120	3	96.55
5	15	Fact	8	60	5	93.34
19	16	Center	10	120	3	96.43
14	17	Axial	10	120	5	96.65
18	18	Center	10	120	3	95.99
3	19	Fact	8	180	1	86.43
4	20	Fact	12	180	1	88.5

Table 3: *Sequential Model Sum of Squares.*

Source	Sum of Squares	df	Mean Square	F Value	p-value (Prob >F)	
Mean vs Total	173976.5	1	173976.5311	-	-	-
Linear vs Mean	258.9811	3	86.32703333	8.097154	0.0017	-
2FI vs Linear	5.085637	3	1.6952125	0.133161	0.9386	-
Quadratic vs 2FI	162.6379	3	54.21263561	189.6256	<0.0001	Suggested
Cubic vs Quadratic	1.0874	4	0.27185	0.920729	0.5094	Aliased
Residual	1.771531	6	0.295255114	-	-	-
Total	174406.1	20	8720.304735	-	-	-

The suggestion of the quadratic model in Table 4 stems from its balance between fit and simplicity. The quadratic model captures the necessary complexity without overfitting, as indicated by the non-significant lack of fit test. It offers a reliable representation of the underlying process for biodiesel production, thus making it a preferable choice over the cubic model, which, despite its lower residual SS, demonstrates significant lack of fit issues, making it less reliable for predictive purposes. Also, in

Table 4: *Lack of Fit Tests.*

Model Type	Sum of Squares	df	Mean Square	F Value	p-value (Prob >F)	
Linear	170.0813	11	15.46193864	154.2646	<0.0001	-
2FI	164.9957	8	20.62446094	205.7713	<0.0001	-
Quadratic	2.357781	5	0.471556136	4.70474	0.0572	Suggested
Cubic	1.270381	1	1.270380682	12.67466	0.0162	Aliased
Pure Error	0.50115	5	0.10023	-	-	-

Table 5, the quadratic model stands out with a standard deviation (Std. Dev.) of 0.53469, indicating it fits the data well with low variability. Its R^2 value is 0.9933, suggesting that 99.33% of the variability in the response variable can be explained by this model. This high R^2 value, along with an adjusted R^2 of 0.9874 and a predicted R^2 of 0.9410, confirms the model's robustness and predictive power [55], [56].

Table 5: *Model Summary Statistics.*

Source	Std. Dev.	R^2	Adjusted R^2	Predicted R^2	PRESS	
Linear	3.265181	0.602894	0.528436067	0.32497	289.9685	-
2FI	3.567986	0.614733	0.436916891	-1.35097	1009.891	-
Quadratic	0.53469	0.993345	0.987354681	0.940979	25.35346	Suggested
Cubic	0.543374	0.995876	0.986940589	-2.63525	1561.571	Aliased

In Table 5, the Prediction Error Sum of Squares (PRESS) value for the quadratic model is 25.35346, further demonstrating its accuracy in prediction. These statistics collectively suggest that the quadratic model is highly suitable for optimizing FAME production conditions compared to other models such as Linear or 2FI, which show lower R^2 values and higher standard deviations, indicating less precision and reliability.

3.4 ANOVA, Fit Statistics and Coefficient Estimate

As evidenced in Table 6, the model's overall SS is 426.7046, with an MS of 47.41163, resulting in a highly significant F value of 165.8369 ($p < 0.0001$). This indicates that the quadratic model is highly significant [57]. Breaking down the individual components, factor C has the highest SS (230.496), MS (230.496), and an extremely high F value (806.2315) with a p-value < 0.0001, demonstrating it as the most influential factor in the model. Factor B also shows substantial influence with an SS of 25.76025, MS of 25.76025, F value of 90.10449, and a p-value < 0.0001. Factor A has an SS of 2.72484, MS of 2.72484, F value of 9.530976, and a significant p-value of 0.0115, indicating it is as also important but to a lesser extent.

Moreso, interactions such as AB and AC show varying significance, with AB having an F value of 4.228898 and a p-value of 0.0668, and AC having an F value of 11.06222 with a p-value of 0.0077, indicating significant interaction effects on the response. The quadratic terms A2, B2, and C2 are all significant with high F values and very low p-values, confirming the non-linear effects of these factors. Additionally, the residual SS is low at 2.858931, with an MS of 0.285893, indicating good model fit. Lastly, the lack of fit is not significant (F value = 4.70474, p-value = 0.0572 – Table 6), suggesting that the model adequately captures the data variability without significant error. In Table 7, the C.V.% or Coefficient of Variation is 0.5733%, indicating that the model is highly reliable and precise, as lower C.V.% values signify higher precision and consistency in the data [45, 60]. This low value implies minimal variation relative to the mean, making the model's predictions stable and

Table 6: *ANOVA Response Surface for the Quadratic Model Chosen.*

Source	Sum of Squares	df	Mean Square	F Value	p-value (Prob >F)	
Model	426.7046	9	47.41163	165.8369	<0.0001	significant
A	2.72484	1	2.72484	9.530976	0.0115	-
B	25.76025	1	25.76025	90.10449	<0.0001	-
C	230.496	1	230.496	806.2315	<0.0001	-
AB	1.209012	1	1.209012	4.228898	0.0668	-
AC	3.162612	1	3.162612	11.06222	0.0077	-
BC	0.714012	1	0.714012	2.497481	0.1451	-
A2	4.029301	1	4.029301	14.09373	0.0038	-
B2	23.36008	1	23.36008	81.70916	<0.0001	-
C2	49.77818	1	49.77818	174.1147	<0.0001	-
Residual	2.858931	10	0.285893	-	-	-
Lack of Fit	2.357781	5	0.471556	4.70474	0.0572	not significant
Pure Error	0.50115	5	0.10023	-	-	-
Cor Total	429.5636	19	-	-	-	-

trustworthy.

Table 7: *Fit Statistics.*

Metric	Value
Std. Dev.	0.53469
Mean	93.2675
C.V. %	0.573286
PRESS	25.35346
R^2	0.993345
Adj. R^2	0.987355
Predicted R^2	0.940979
Adeq. Prec.	42.14776

Adequate precision is 42.14776 in Table 7, far exceeding the threshold value of 4. This metric measures the signal-to-noise ratio, and a value above 4 is desirable as it indicates an adequate signal [59]. A high adequate precision value suggests that the model can be used to navigate the design space effectively [45], ensuring the predictions are reliable and can guide experimental conditions confidently. Table 8 presents the coefficient estimates and Confidence Intervals (CI) for the quadratic model applied in the study. The intercept boasts a coefficient estimate of 96.24682 with a remarkably low standard error of 0.183813, underscoring the model's high degree of precision. Its 95% CI ranges narrowly from 95.83726–96.65638, showing that it is reliable. Factor A, representing the methanol–oil ratio, has a coefficient estimate of 0.522 with a standard error of 0.169084. Its 95% CI spans from 0.145258–0.898742, indicating a positive and statistically significant impact on biodiesel conversion [40, 62]. Factor B, which denotes reaction time, shows a more substantial positive influence with a coefficient estimate of 1.605 and a CI extending from 1.228258–1.981742.

Most notably, Factor C, representing catalyst load, exhibits the highest positive coefficient estimate of 4.801, with its CI ranging from 4.424258–5.177742, underscoring its profound effect on the biodiesel conversion process. Interaction terms AB, AC, and BC show negative coefficients in Table 8, suggesting that the interactions between these factors negatively affect biodiesel conversion

Table 8: *Coefficient Estimate and Confidence Interval.*

Factor	Coefficient Estimate	df	Standard Error	95% CI Low	95% CI High	VIF
Intercept	96.24682	1	0.183813	95.83726	96.65638	-
A	0.522	1	0.169084	0.145258	0.898742	1
B	1.605	1	0.169084	1.228258	1.981742	1
C	4.801	1	0.169084	4.424258	5.177742	1
AB	-0.38875	1	0.189041	-0.80996	0.03246	1
AC	-0.62875	1	0.189041	-1.04996	-0.20754	1
BC	-0.29875	1	0.189041	-0.71996	0.12246	1
A2	1.210455	1	0.32243	0.492036	1.928873	1.818182
B2	-2.91455	1	0.32243	-3.63296	-2.19613	1.818182
C2	-4.25455	1	0.32243	-4.97296	-3.53613	1.818182

[31]. While the quadratic terms A^2, B^2, and C^2 have significant impacts, particularly B^2 and C^2 with negative coefficients of -2.91455 and -4.25455, respectively. VIF stands for Variance Inflation Factor [61]. The VIF values for all terms are low, indicating no multicollinearity issues among the predictors.

3.5 Two Variables Response Contour Plots

Figure (4a-6a) contour plots uses color gradients to represent different levels of FAME conversion efficiency, with distinct lines marking changes in conversion percentages. Alternatively, the surface plot or Figure (4b-6b) visualizes these data points in a 3D space, using color and elevation to denote conversion efficiency at varying combinations of 2 variables. An example is A (methanol-oil ratio) and B (reaction time) in Figure 4. The color patterns range from cool to warm tones, indicating lower to higher biodiesel conversion rates. Optimal combination identified in Figure 4, where both methanol-oil ratio and reaction time result in maximum biodiesel conversion [62], is approximately at a methanol-oil ratio of 11 and a reaction time of 120 min. This particular combination corresponds to a biodiesel conversion rate close to 98.2%, highlighting the most efficient conditions for the reaction under study.

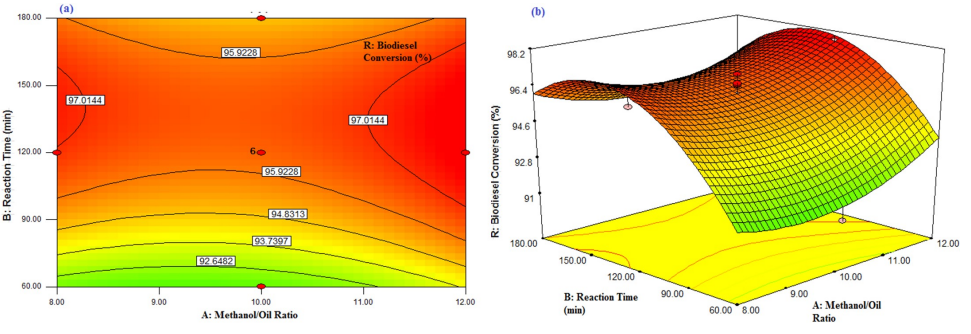

Figure 4: *Biodiesel Conversion Versus A-B (a) Contour and (b) Surface Plots.*

Normally, the optimal combination of variables can be determined by locating the highest peak on the surface plot or the innermost contour line on the contour plot, indicating the maximum FAME conversion percentage. In view of that, the optimal combination derived from Figure 5 shows that a methanol-oil ratio (A) of approximately 11.5 and a catalyst load (C) of about 3.5 wt.% result in a

biodiesel conversion rate of around 98.57% (higher than A-B choice of value). Researchers discovered a phenomenon they described as 'molar ratio limitation' beyond which biodiesel production will be reduced as well as the fuel purity [34]. In this study, the threshold value is between 11.0–11.5, derived from Figures 4 and 5. In Figure 5 illustrated previously, the colors range from dark blue to red, with dark blue representing the lowest conversion rates and red representing the highest [63].

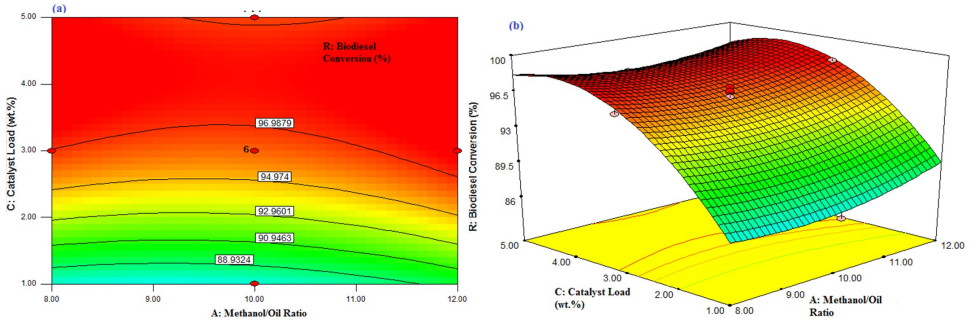

Figure 5: *Biodiesel Conversion Versus A-C (a) Contour and (b) Surface Plots.*

As such, the optimal combination of Factor A and Factor C for achieving the highest biodiesel conversion is highlighted in the red region. However, the 3D surface in more clearly pinpoint the optimal combinations than in this study, due to a smoother curvature [64]. A 98.57% FAME conversion relative to A and C is consistent with the requirements of the European Standard EN-14214 [66-68]. A-C relationship with % FAME conversion have been reported severally [52], [68], [69], [70], and was generally discovered that an individual or simultaneous increase in A and C results in concurrent rise in biodiesel conversion. Figure 6 shows the optimal combination of reaction time (B) and catalyst load (C) for biodiesel conversion. It is observed that the optimal combination is at approximately 4.5% catalyst load and 135 min of reaction time, yielding the highest biodiesel conversion rate of around 98%. The umbrella shape showcased by all the surface plots suggests that there is a single optimal combination of the two input variables where the response variable reaches its maximum. As we move away from this optimal point in any direction within the plotted range, the response variable decreases. The curvature of the umbrella shape indicates the sensitivity of the response variable to changes in the input variables, as presented using identical factors [34], [68], [71]. Steeper slopes near the peak imply greater sensitivity [15], meaning small changes in the input variables around the optimal point can significantly impact the response variable.

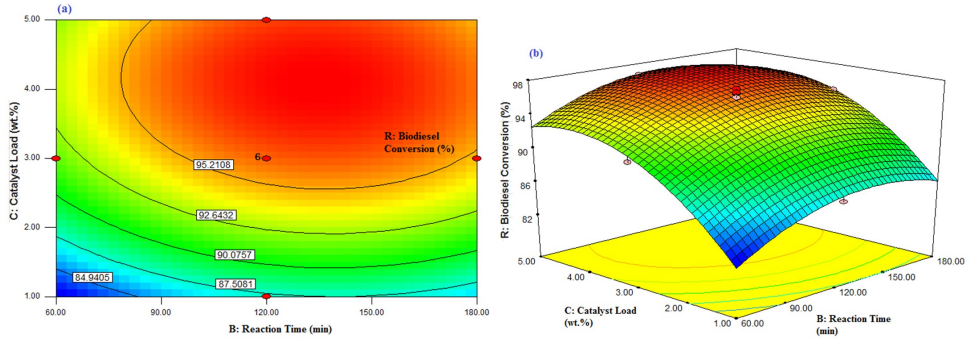

Figure 6: *Biodiesel Conversion Versus B-C (a) Contour and (b) Surface Plots.*

Based on Figures 4, 5, and 6, the best combination for efficient resource utilization and maximum

biodiesel conversion is from Figure 5. It is ranked first due to its high efficiency and moderate catalyst usage. Figure 4 ranks second, because it has less optimized catalyst load. Figure 6 ranks third, due to the fact that it requires higher catalyst usage and longer reaction time, making it less resource-efficient. Thus, lower reaction period of 90 minutes [72] and 51 min [67] are more advantageous. In terms of the polynomial model used in RSM, an umbrella-shaped surface typically corresponds to a second-order response surface [37]. This implies that the relationship between the response and the input variables (A, B and C) can be adequately described by a quadratic equation, capturing both linear and interaction effects of the variables.

3.6 Model Equation for FAME Conversion and Fit

Base on Equation 3 and Equation 4 in terms of coded and actual factors, the predicted biodiesel conversion efficiency was computed by Design Expert for the 20 observations in Table 2.

$$\text{FAME Conv. } (\%)_{\text{Coded}} = 96.24682 + 0.522\,A + 1.605\,B + 4.801C - 0.38875AB - 0.62875\,AC - 0.29875\,BC + 1.210455\,A^2 - 2.91455\,B^2 - 4.25455C^2 \quad (3)$$

$$\text{FAME Conv. } (\%)_{\text{Actual}} = 82.7564 - 4.93096\,A + 0.260918\,B + 10.65294C - 0.00324AB - 0.15719\,AC - 0.00249\,BC + 0.302614\,A^2 - 0.00081\,B^2 - 1.06364C^2 \quad (4)$$

The predicted versus actual response plot is as shown in Figure 7a with an R^2 value of 0.9933. This strong performance of the quadratic model is crucial for achieving high conversions and efficient biodiesel production, as it accurately captures the relationship between process variables and the response, facilitating better optimization and control of the production process. As clearly explained [66], [73], Figure 7b point to the distribution between the predicted versus experimental studentized residuals and exposed the normal distribution of studentized residuals vis-à-vis to S-shape curve was not completely formed.

There are several 3 variable combinations suggested by the CCD-RSM Design Expert that would give maximum FAME conversion, as shown in Table 9. Design Expert selected row number 1 as the optimal combination because it achieves a high biodiesel conversion rate of 97.83%, which is close to the highest among the options provided. This combination of methanol-oil ratio (A = 10.57), reaction time (B = 126.67 min), and catalyst load (C = 4.24 wt.%) also meets all experimental constraints and has a desirability score of 1, indicating it satisfies all criteria set by the current study effectively.

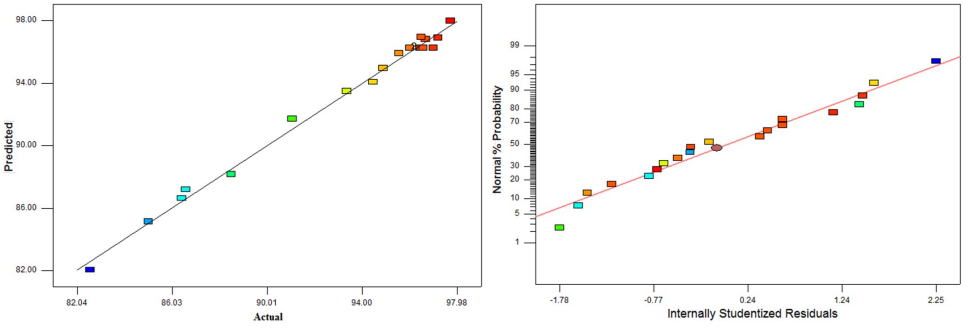

Figure 7: *(a) Predicted Versus Actual Biodiesel Conversion and (b) Normal Plot of Residuals.*

There are several 3 variable combinations suggested by the CCD-RSM Design Expert that would give maximum FAME conversion, as shown in Table 9. Design Expert selected row number 1

as the optimal combination because it achieves a high biodiesel conversion rate of 97.83%, which is close to the highest among the options provided. This combination of methanol-oil ratio (A = 10.57), reaction time (B = 126.67 min), and catalyst load (C = 4.24 wt.%) also meets all experimental constraints and has a desirability score of 1, indicating it satisfies all criteria set by the current study effectively.

Table 9: *Desirability and Optimal Combinations*

Number	A	B (min)	C (wt.%)	Response (%)	Desirability	
1	10.57	126.67	4.24	97.8301	1	Selected
2	11.42	144.46	3.41	97.97371	1	-
3	11.96	122.01	3.36	98.56847	1	-

Because lower CH_3OH/oil ratios are generally more resource-efficient as they use less CH_3OH. Also, lower ratios are typically safer as CH_3OH is toxic and flammable. Short reaction times are more efficient in terms of energy and time resources. Considering all factors, Combination 1 offers a balanced approach with good resource efficiency and environmental safety, and a high conversion, despite the higher catalyst load. Combination 3 provides the highest conversion and best reaction time but at the cost of higher CH_3OH usage, which could be less environmentally friendly. Combination 2 falls in between, offering moderate benefits but the least resource-efficient reaction time.

4. Conclusion

This study positively explored the use of sulfonated DPS as a catalyst for the esterification of PA to produce biodiesel, utilizing two characterization methods and RSM optimization. It is observed that while hydroxyl group contributed to the overall functionality of the DPS catalyst, their impact is less compared to sulfonic and carbonyl groups. In addition, aliphatic C-H stretching groups are more common and less critical to the specific catalytic activity required for biodiesel production, as revealed by the FTIR. Basically, FTIR revealed the presence of sulfonic acid groups, which are essential for the acidic properties and catalytic efficiency of the catalyst, while AFM showed a moderately rough surface with significant peaks and valleys, providing ample active sites for the esterification reaction. The optimization process conducted using CCD within the Design Expert software, showed that the optimal conditions for the esterification process are a methanol-to-oil ratio of 10.57:1, a reaction time of 127 min, and a catalyst load of 4.24 wt.%. Under these conditions, the biodiesel conversion rate reached an impressive 97.83%, demonstrating the high efficiency of the sulfonated DPS catalyst. It is almost in consonance with an observed value of 98.01%. A reusability test should be done in order to ascertain the catalyst effectiveness in subsequent runs of the biodiesel production.

References

[1] U. I. Gaya, E. Otene, and A. H. Abdullah, "Adsorption of aqueous Cd(II) and Pb(II) on activated carbon nanopores prepared by chemical activation of doum palm shell," Springerplus, vol. 4, no. 458, pp. 1–18, 2015, doi: 10.1186/s40064-015-1256-4.

[2] I. M. Muhammad, A. Y. Abdulkarim, and S. Adamu, "Characterization of doum palm seed kernel as natural sorbent for metal ions removal from Gombe ternary wastewater," Path Sci. Int. Electron. Sci. J., vol. 5, no. 7, pp. 2001–2008, 2019, doi: 10.22178/pos.48-2.

[3] M. I. Alkali et al., "Adsorption of Pb (II) ion onto Modified Doum Palm (Hyphaene thebaica) Shells: Isotherm, Kinetic and Thermodynamic Studies," Arid Zo. J. Basic Appl. Res., vol. 1, no. 5, pp. 80-102, 2022, doi: 10.55639/607gfedc.

[4] S. Zannen, L. Ghali, M. T. Halimi, and M. Ben Hssen, "Effect of chemical extraction on physicochemical and mechanical properties of doum palm fibres," Adv. Mater. Phys. Chem., vol.

4, no. 10, 2014.
[5] S. A. Seth, I. S. Aji, and A. Tokan, "Effects of particle size and loading on tensile and flexural properties of polypropylene reinforced doum palm shell particles composites," Am. Sci. Res. J. Eng. Technol. Sci., vol. 44, no. 1, pp. 231–239, 2018.
[6] A. Z. Liman, T. Adagba, and H. A. Umar, "Effect of crushed doum palm shell as partial replacement of coarse aggregate in concrete," FUDMA J. Sci., vol. 4, no. 4, pp. 1–9, 2020, doi: 10.33003/fjs-2020-0404-45.
[7] M. O. Nwabueze, A. Khaleel, and M. Abdulhameed, "Investigating the performance of Doum Palm Shell as an aggregate for making lightweight interlocking blocks," IEEE Conf. Proc. (IEEE Conf Proc), vol. 2023, no. ICMEAS, pp. 1–5, 2023.
[8] R. A. Kyari, I. S. Aji, and M. Dauda, "Determination of the tensile strength and flexural strength of polypropylene filled Doum Palm Shell particles and sugarcane bagasse composite," Int. J. Information, Eng. Technol., vol. 12, no. 7, pp. 40–50, 2024, doi: 10.4272-1454-381-1276.
[9] A. K. Aremu and O. K. Fadele, "Moisture dependent thermal properties of doum palm fruit (Hyphaene Thebaica)," J. Emerg. Trends Eng. Appl. Sci., vol. 1, no. 2, pp. 199–204, 2010.
[10] D. M. Kongnine, P. Kpelou, N. Attah, and E. Mouzou, "Evaluation of energy properties of mixed biomass charcoal derived from coconut, palmyra palm nuts and doum palm nuts shells," Sci. J. Energy Eng., vol. 9, no. 2, pp. 17–21, 2021, doi: 10.11648/j.sjee.20210902.11.
[11] D. S. Nouhou, A. Ali, H. G. Ibrahim, and M. Boukar, "Study of mass and energy yields of an agroforestry residues carbonizer," Int. J. Eng. Trends Technol., vol. 69, no. 11, pp. 53–60, 2021, doi: 10.14445/22315381/IJETT-V69I11P207.
[12] A. M. Abubakar, H. M. Kefas, Y. Luka, and J. J. Kawuwa, "Revolutionalizing biodiesel synthesis: Kinetic and thermodynamic insights with carbonized doum-shell catalyst," Trends Ecol. Indoor Environ. Eng., vol. 2, no. 2, pp. 11–23, 2024, doi: 10.62622/TEIEE.024.2.2.11-23.
[13] S. Ban, R. Shrestha, Y. Chaudhary, J.-K. Jeon, R. Joshi, and B. Uprety, "Process simulation and economic analysis of dolomite catalyst based biodiesel production from Nepalese Jatropha Curcas," Clean. Chem. Eng., vol. 2, no. 100029, pp. 1–8, 2022, doi: 10.1016/j.clce.2022.100029.
[14] H. I. Mohammed, K. Garba, S. I. Ahmed, and L. G. Abubakar, "Thermodynamics and kinetics of Doum (Hyphaene thebaica) shell using thermogravimetric analysis: A study on pyrolysis pathway to produce bioenergy," Renew. Energy, vol. 200, pp. 1275–1285, 2022, doi: 10.1016/j.renene.2022.10.042.
[15] S. M. S. Ardebili, T. T. Hashjin, B. Ghobadian, G. Najafi, S. Mantegna, and G. Cravotto, "Optimization of biodiesel synthesis under simultaneous ultrasound-microwave irradiation using response surface methodology (RSM)," Green Process Synth., vol. 4, pp. 259–267, 2015, doi: 10.1515/gps-2015-0029.
[16] T. Khan, "Applications of Atomic Force Microscopy in materials characterization," Azo Materials, pp. 1–5, May 2024.
[17] M. A. Waheed, O. D. Samuel, B. O. Bolaji, and O. U. Dairo, "RSM based optimization of biodiesel production from tobacco seed oil," in Renewable Energy and Sustainable Development, R. T. D. Prabhakaran and S. A. Kale, Eds., Nova Science Publishers, Inc, 2015, pp. 13–15.
[18] M. Rahimi, B. Aghel, M. Alitabar, A. Sepahvand, and H. R. Ghasempour, "Optimization of biodiesel production from soybean oil in a microreactor," Energy Convers. Manag., vol. 79, pp. 599–605, 2014, doi: 10.1016/j.enconman.2013.12.065.
[19] M. W. Mumtaz, H. Mukhtar, F. Anwar, and N. Saari, "RSM based optimization of chemical and enzymatic transesterification of palm oil: Biodiesel production and assessment of exhaust emission levels," Sci. World J., vol. 2014, no. 526105, pp. 1–11, 2014, doi: 10.1155/2014/526105.
[20] M. Mir and S. M. Ghoreishi, "Response surface optimization of biodiesel production via catalytic transesterification of fatty acids," Chem. Eng. Technol., vol. 38, no. 00, pp. 1–10, 2015, doi: 10.1002/ceat.201300328.

[21] M. W. Mumtaz et al., "Response Surface Methodology: An emphatic tool for optimized biodiesel production using rice bran and sunflower oils," Energies, vol. 5, pp. 3307–3328, 2012, doi: 10.3390/en5093307.
[22] C. N. Njoku and S. K. Otisi, "Application of Central Composite Design with Design Expert v13 in process optimization," in Response Surface Methodology-Research advances and applications, P. Kayarogannam, Ed., InTech Open, 2023. doi: 10.5772/intechopen.109704.
[23] K. Boonmee, S. Chuntranuluck, V. Punsuvon, and P. Silayoi, "Optimization of biodiesel production from jatropha oil (Jatropha curcas L.) using Response Surface Methodology," Kasetsart J. (Natural Sci., vol. 44, no. 2, pp. 290–299, 2010.
[24] E. Betiku and S. O. Ajala, "Modeling and optimization of Thevetia peruviana (yellow oleander) oil biodiesel synthesis via Musa paradisiacal (plantain) peels as heterogeneous base catalyst: A case of artificial neural network vs. response surface methodology," Ind. Crop. Prod., vol. 53, pp. 314–322, 2014, doi: 10.1016/j.indcrop.2013.12.046.
[25] A. K. Aremu and O. K. Fadele, "Study of some properties of doum palm fruit (Hyphaene thebaica Mart.) in relation to moisture content," African J. Agric. Res., vol. 6, no. 15, pp. 3597–3602, 2011, doi: 10.5897/AJAR11.247.
[26] S. Samaila, H. M. Adamu, and J. J. Deshi, "Adsorption of lead and mercury ions on chemically treated doum palm shells," IDOSR J. Sci. Res., vol. 2, no. 1, pp. 25–36, 2017.
[27] A. U. Babuje, I. S. Diso, and A. A. Adamu, "Statistical optimization of process parameters of the synthesis of bio-char from Doum Palm Shell (DPS) for used as activated carbon," Iconic Res. Eng., vol. 7, no. 5, pp. 106–113, 2023.
[28] H. M. Kefas, R. Yunus, U. Rashid, and Y. H. Taufiq-Yap, "Enhanced biodiesel synthesis from palm fatty acid distillate and modified sulfonated glucose catalyst via an oscillation flow reactor system," J. Environ. Chem. Eng., vol. 7, no. 2, pp. 1–10, 2019, doi: 10.1016/j.jece.2019.102993.
[29] A. A. Jazie, H. Pramanik, A. S. K. Sinha, and A. A. Jazie, "Egg shell as eco-friendly catalyst for transesterification of rapeseed oil: Optimization for biodiesel production," Spec. Issue Int. J. Sustain. Dev. Green Econ., vol. 2, no. 1, pp. 27–32, 2013.
[30] A. H. M. Fauzi and N. A. Saidina Amin, "Optimization of oleic acid esterification catalyzed by ionic liquid for green biodiesel synthesis," Energy Convers. Manag., vol. 76, pp. 818–827, 2013, doi: 10.1016/j.enconman.2013.08.029.
[31] Y. C. Wong, Y. P. Tan, Y. H. Taufiq-Yap, and I. Ramli, "An optimization study for transesterification of palm oil using Response Surface Methodology (RSM)," Sains Malaysiana, vol. 44, no. 2, pp. 281–290, 2015.
[32] H. Yu et al., "An efficient heterogeneous acid catalyst derived from waste ginger straw for biodiesel production," Renew. Energy, vol. 176, pp. 533–542, 2021,
doi: 10.1016/j.renene.2021.05.098.
[33] H. M. Kefas, R. Yunus, U. Rashid, and Y. H. Taufiq-Yap, "Modified sulfonation method for converting carbonized glucose into solid acid catalyst for the esterification of palm fatty acid distillate," Fuel, vol. 229, pp. 68–78, 2018, doi: 10.1016/j.fuel.2018.05.014.
[34] E. Fayyazi, B. Ghobadian, G. Najafi, B. Hosseinzadeh, R. Mamat, and J. Hosseinzadeh, "An ultrasound-assisted system for the optimization of biodiesel production from chicken fat oil using a genetic algorithm and response surface methodology," Ultrason. Sonochem., vol. 26, pp. 312–320, 2015, doi: 10.1016/j.ultsonch.2015.03.007.
[35] P. J. García-moreno, M. Khanum, A. Guadix, and E. M. Guadix, "Optimization of biodiesel production from waste fish oil," Renew. Energy, vol. 68, pp. 618–624, 2014,
doi: 10.1016/j.renene.2014.03.014.
[36] S. Awad, M. Paraschiv, E. G. Varuvel, and M. Tazerout, "Optimization of biodiesel production from animal fat residue in wastewater using response surface methodology," Bioresour. Technol., vol. 129, pp. 315–320, 2013, doi: 10.1016/j.biortech.2012.11.086.

[37] S. M. Ghoreishi and P. Moein, "Biodiesel synthesis from waste vegetable oil via transesterification reaction in supercritical methanol," J. Supercrit. Fluids, vol. 76, pp. 24–31, 2013, doi: 10.1016/j.supflu.2013.01.011.
[38] M. S. Ahamed, P. Lingfa, and M. Chandrasekaran, "RSM modelling and optimization for performance evaluation of biodiesel production process from livistona jenkinsiana using NaOH as a catalyst," Eng. Res. Express, vol. 5, no. 4, pp. 1–13, 2023, doi: 10.1088/2631-8695/ad069b.
[39] H. M. Kefas, R. Yunus, U. Rashid, and Y. H. Taufiq-yap, "Modified sulfonated glucose-catalyzed esterification of palm fatty acid distillate: Kinetics and fuel properties," Am. J. Chem. Eng., vol. 8, no. 6, pp. 131–138, 2020, doi: 10.11648/j.ajche.20200806.12.
[40] H. V. Kamath, I. Regupathi, and M. B. Saidutta, "Optimization of two step karanja biodiesel synthesis under microwave irradiation," Fuel Process. Technol., vol. 92, no. 1, pp. 100–105, 2011, doi: 10.1016/j.fuproc.2010.09.003.
[41] H. V Lee, R. Yunus, J. C. Juan, and Y. H. Taufiq-Yap, "Process optimization design for jatropha-based biodiesel production using response surface methodology," Fuel Process. Technol., vol. 92, pp. 2420–2428, 2011, doi: 10.1016/j.fuproc.2011.08.018.
[42] G. F. Silva, F. L. Camargo, and A. L. O. Ferreira, "Application of response surface methodology for optimization of biodiesel production by transesterification of soybean oil with ethanol," Fuel Process. Technol., vol. 92, pp. 407–413, 2011, doi: 10.1016/j.fuproc.2010.10.002.
[43] M. Sabzimaleki, B. Ghobadian, M. M. Farsibaf, G. Najafi, M. D. Soufi, and S. M. S. Ardebili, "Optimization of biodiesel ultrasound-assisted synthesis from castor oil using Response Surface Methodology (RSM)," Chem. Prod. Process Model., vol. 10, no. 2, pp. 123–133, 2015, doi: 10.1515/cppm-2014-0013.
[44] A. S. Yusuff, K. A. Thompson-Yusuff, and J. Porwal, "Sulfonated biochar catalyst derived from eucalyptus tree shed bark: Synthesis, characterization and its evaluation in oleic acid esterification," RSC Adv., vol. 12, pp. 10237–10248, 2022, doi: 10.1039/d1ra09179d.
[45] T. Tamoradi, A. R. Kiasat, H. Veisi, V. Nobakht, and B. Karmakar, "RSM process optimization of biodiesel production from rapeseed oil and waste corn oil in the presence of green and novel catalyst," Sci. Rep., vol. 12, no. 19652, pp. 1–15, 2022, doi: 10.1038/s41598-022-20538-4.
[46] A. P. da L. Correa, R. R. C. Bastos, G. N. da R. Filho, J. R. Zamian, and L. R. Da Conceicao, "Preparation of sulfonated carbon-based catalysts from murumuru kernel shell and their performance in the esterification reaction," RSC Adv., vol. 10, pp. 20245–20256, 2020, doi: 10.1039/d0ra03217d.
[47] C. Tcheka, M. M. Conradie, V. A. Assinale, and J. Conradie, "Mesoporous biochar derived from Egyptian doum palm (Hyphaene thebaica) shells as low-cost and biodegradable adsorbent for the removal of methyl orange dye: Characterization, kinetic and adsorption mechanism," Chem. Phys. Impact, vol. 8, no. 100446, pp. 1–12, 2024, doi: 10.1016/j.chphi.2023.100446.
[48] M. McDonough, "Data processing analysis for Atomic Force Microscopy (AFM)," Bachelor of Science Undergraduate Theses and Capstone Projects, Physics Department, Suffolk University, 2020.
[49] M. A. S. Quintanilla, "Surface analysis using contact mode AFM," in Encyclopedia of Tribology, Q. J. Wang and Y.-W. Chung, Eds., Springer, Boston, MA, 2013, pp. 3401–3411. doi: 10.1007/978-0-387-92897-5-323.
[50] R. Rezaei, M. Mohadesi, and G. R. Moradi, "Optimization of biodiesel production using waste mussel shell catalyst," Fuel, vol. 109, pp. 534–541, 2013, doi: 10.1016/j.fuel.2013.03.004.
[51] E. Betiku, O. R. Omilakin, S. O. Ajala, A. A. Okeleye, A. E. Taiwo, and B. O. Solomon, "Mathematical modeling and process parameters optimization studies by artificial neural network and response surface methodology: A case of non-edible neem (Azadirachta indica) seed oil biodiesel synthesis," Energy, vol. XXX, pp. 1–8, 2014, doi: 10.1016/j.energy.2014.05.033.
[52] M. Saqib, M. W. Mumtaz, A. Mahmood, and M. I. Abdullah, "Optimized biodiesel produc-

tion and environmental assessment of produced biodiesel," Biotechnol. Bioprocess Eng., vol. 17, pp. 617–623, 2012, doi: 10.1007/s12257-011-0569-6.
[53] Y. Yücel, "Optimization of biocatalytic biodiesel production from pomace oil using response surface methodology," Fuel Process. Technol., vol. 99, pp. 97–102, 2012, doi: 10.1016/j.fuproc.2012.02.008.
[54] T. Muppaneni et al., "Optimization of biodiesel production from palm oil under supercritical ethanol conditions using hexane as co-solvent: A response surface methodology approach," Fuel, vol. 107, pp. 633–640, 2013, doi: 10.1016/j.fuel.2012.11.046.
[55] H. Hamze, M. Akia, and F. Yazdani, "Optimization of biodiesel production from the waste cooking oil using response surface methodology," Process Saf. Environ. Prot., pp. 1–36, 2014, doi: 10.1016/j.psep.2014.12.005.
[56] M. I. Jahirul, W. Koh, R. J. Brown, W. Senadeera, I. O'Hara, and L. Moghaddam, "Biodiesel production from non-edible beauty leaf (Calophyllum inophyllum) oil: Process optimization using Response Surface Methodology (RSM)," Energies, vol. 7, pp. 5317–5331, 2014, doi: 10.3390/en7085317.
[57] L. B. Umdagas, H. Umar, A. M. Abubakar, and Z. A. Turajo, "Optimization of biodiesel from Citrillus lantanus seed oil using alkali-catalyzed methanolysis," Int. J. Sci. Res. Chem. Sci., vol. 9, no. 5, pp. 14–19, 2022.
[58] A. S. Reshad, P. Tiwari, and V. V Goud, "Extraction of oil from rubber seeds for biodiesel application: Optimization of parameters," Fuel, vol. xxx, pp. 1–9, 2015, doi: 10.1016/j.fuel.2015.02.058.
[59] H. S. Pali, N. Kumar, Y. Alhassan, and A. Deep, "Process optimization of biodiesel production from Sal seed oil using Response Surface Methodology [RSM] and diesel," SAE Int., pp. 1–9, 2015, doi: 10.4271/2015-01-1297.
[60] E. Betiku, S. S. Okunsolawo, S. O. Ajala, and O. S. Odedele, "Performance evaluation of artificial neural network coupled with generic algorithm and response surface methodology in modeling and optimization of biodiesel production process parameters from shea tree (Vitellaria paradoxa) nut butter," Renew. Energy, vol. 76, pp. 408–417, 2015, doi: 10.1016/j.renene.2014.11.049.
[61] K. Feldman, "Using Variance Inflation Factor to optimize regression models," iSixSigma.
[62] B. Salamatinia, H. Mootabadi, S. Bhatia, and A. Z. Abdullah, "Optimization of ultrasonic-assisted heterogeneous biodiesel production from palm oil: A response surface methodology approach," Fuel Process. Technol., vol. 91, pp. 441–448, 2010, doi: 10.1016/j.fuproc.2009.12.002.
[63] M. Mansourpoor and A. Shariati, "Optimization of biodiesel production from sunflower oil using Response Surface Methodology," J. Chem. Eng. Process Technol., vol. 3, no. 5, pp. 1–6, 2012, doi: 10.4172/2157-7048.1000141.
[64] A. Abuhabaya, J. Fieldhouse, and D. Brown, "The optimization of biodiesel production by using response surface methodology and its effect on compression ignition engine," Fuel Process. Technol., vol. 113, pp. 57–62, 2013, doi: 10.1016/j.fuproc.2013.03.025.
[65] M. Flota-Bañuelos et al., "Obtaining biodiesel from seeds of Ricinus communis: methodological proposal," Int. J. Oil, Gas Coal Technol., vol. 29, no. 4, pp. 408–425, 2022, doi: 10.1504/IJOGCT.2022.121264.
[66] I. Noshadi, N. A. S. Amin, and R. S. Parnas, "Continuous production of biodiesel from waste cooking oil in a reactive distillation column catalyzed by solid heteropolyacid: Optimization using response surface methodology (RSM)," Fuel, vol. 94, pp. 156–164, 2012, doi: 10.1016/j.fuel.2011.10.018.
[67] V. Makareviciene, V. Skorupskaite, D. Levisauskas, V. Andruleviciute, and K. Kazancev, "The optimization of biodiesel fuel production from microalgae oil using Response Surface Methodology," Int. J. Green Energy, pp. 37–41, 2013, doi: 10.1080/15435075.2013.777911.
[68] W. N. N. Wan Omar and N. A. S. Amin, "Optimization of heterogeneous biodiesel production from waste cooking palm oil via response surface methodology," Biomass and Bioenergy,

vol. 35, no. 3, pp. 1329–1338, 2011, doi: 10.1016/j.biombioe.2010.12.049.
[69] E. Rashtizadeh, F. Farzaneh, and Z. Talebpour, "Synthesis and characterization of Sr3Al2O6 nanocomposite as catalyst for biodiesel production," Bioresour. Technol., vol. 154, pp. 32–37, 2014,
doi: 10.1016/j.biortech.2013.12.014.
[70] S. Pradhan, C. S. Madankar, P. Mohanty, and S. N. Naik, "Optimization of reactive extraction of castor seed to produce biodiesel using response surface methodology," Fuel, vol. 97, pp. 848–855, 2012, doi: 10.1016/j.fuel.2012.02.052.
[71] I. Worapun, K. Pianthong, and P. Thaiyasuit, "Optimization of biodiesel production from crude palm oil using ultrasonic irradiation assistance and response surface methodology," J. Chem. Technol. Biotechnol., vol. 87, pp. 189–197, 2012, doi: 10.1002/jctb.2679.
[72] F. Ferella, G. M. Di Celso, I. De Michelis, V. Stanisci, and F. Vegliò, "Optimization of the transesterification reaction in biodiesel production," Fuel, vol. 89, pp. 36–42, 2010, doi: 10.1016/j.fuel.2009.01.025.
[73] H. Jaliliannosrati, N. A. S. Amin, A. Talebian-Kiakalaieh, and I. Noshadi, "Microwave assisted biodiesel production from Jatropha curcas L. seed by two-step in situ process: Optimization using response surface methodology," Bioresour. Technol., vol. 136, pp. 565–573, 2013, doi: 10.1016/j.biortech.2013.02.078.